Pergamon

Geochimica et Cosmochimica Acta, Vol. 60, No. 22, pp. 4509–4523, 1996

0016-7037/96 $15.00 + .00

PII S0016-7037(96)00256-6

Deep-dwelling planktonic foraminifera of the northeastern Pacific Ocean reveal environmental control of oxygen and carbon isotopic disequilibria

J. D. ORTIZ,* A. C. MIX, W. RUGH, J. M. WATKINS, and R. W. COLLIER
College of Oceanic and Atmospheric Sciences, Oregon State University, Corvallis, OR 97331-5503, USA

(*Received November* 21, 1995; *accepted in revised form July* 8, 1996)

Abstract—We assess the utility of four species of living planktonic foraminifera as tracers of thermocline and intermediate water masses in the northern Pacific Ocean, based on their water-column distribution and shell isotopic composition. Assuming oxygen isotopic equilibria with the water column, we infer apparent calcification depths. This allows an estimate of apparent carbon isotopic disequilibria. We then relax the assumption of oxygen isotopic equilibrium to examine habitat effects on kinetic disequilibrium processes. In the California Current, left-coiling *Neogloboquadrina pachyderma* and *Globigerina calida* calcify in the upper thermocline. *Globorotalia scitula* resides within the Shallow Salinity Minumum (potential density σ_θ = 25.1–26.7), while *Globoquadrina hexagona* is associated with the deeper, North Pacific Intermediate Water (σ_θ = 26.7–26.9). Apparent carbon isotopic disequilibria corrected for oxygen isotopic disequilibria, range from 1.0–1.9‰ in these asymbiotic species. The carbon isotopic disequilibrium can be modeled as a single exponential function of temperature or a logarithmic function of potential food supply. We infer that carbon isotopic disequilibrium increases with metabolic rate, related to temperature and/or food supply. Kinetic processes of oxygen and carbon isotopic disequilibria yields reasonable depth habitats if the slope of the oxygen:carbon isotopic shift is about 0.35, consistent with culture data. Our finding of a link between environment, metabolism, and isotopic disequilibrium observed in oceanic settings suggests the potential to better reconstruct the structure and biological processes of the upper water column from geologic data.

1. INTRODUCTION

Variations in intermediate water properties play a critical role in oceanic nutrient and carbon cycling (e.g., Boyle, 1992). Deep-dwelling planktonic foraminifera are useful as tracers of these variations (Lohmann and Schweitzer, 1990; Schweitzer and Lohmann, 1991; Lohmann, 1992). Because planktonic foraminifera live within the water column rather than in oceanic sediments like their benthic counterparts, they may provide a more direct record of intermediate water variation. Potential problems are changes in a species' depth habitat during ontogeny and isotopic disequilibrium during calcification. Here we assess the utility of four species of planktonic foraminifera as tracers of thermocline and intermediate water masses: *Globorotalia scitula, Globoquadrina hexagona, Globigerina calida,* and left-coiling *Neogloboquadrina pachyderma.* We assess (1) habitats and their relationship to physical and biological processes, and (2) processes of isotopic disequilibrium with the goal of developing more useful paleoceanographic proxies of water mass properties.

We compare the distributions of four species collected with depth-stratified plankton tows from the California Current using the MOCNESS (multiple opening/closing environmental net sensing system) of Wiebe et al. (1985). A first question is whether foraminifera collected on isopycnal surfaces calcified where they were collected. We answer this question by (1) determining whether the individuals possess protoplasm and thus were living or recently living at the time of capture, (2) assessing the distribution of each species along isopycnal surfaces at four tows sites across the California Current, and (3) examining the oxygen and carbon isotopic composition of their shell ($\delta^{18}O_s$ and $\delta^{13}C_s$) compared to equivalent data for the water column ($\delta^{18}O_w$ and $\delta^{13}C_w$) that are translated into predictions for calcite at isotopic equilibrium ($\delta^{18}O_e$ and $\delta^{13}C_e$).

Comparisons of tow depths, oxygen, and carbon isotope data at an array of sites reveals that the foraminifera must be out of equilibrium with the ambient water mass. Using $\delta^{18}O_s$ as a first approximation of calcification depth, we examine patterns of $\delta^{13}C$ disequilibrium and evaluate potential environmental causes. Finally we adjust these estimates by allowing for isotopic disequilibrium in both oxygen and carbon, and find a parsimonious solution that links kinetic processes of isotopic disequilibrium to metabolic processes in real oceanic environments.

2. HYDROGRAPHIC SETTING

The central north Pacific Ocean contains a series of salinity minima between 200 and 1000 m which constitute its intermediate waters. These water masses are shallowest in the north and to the east in the California Current, and deepest to the south and west. The most important of these features are the Shallow Salinity Minumum (SSM: water density (σ_θ) 25.1–26.7) and the North Pacific Intermediate Water (NPIW: σ_θ 26.7–26.9) (e.g., Kenyon, 1978; Yuan and Talley, 1992). In the California Current, the Shallow Salinity Minumum (salinity 32.8–33.9 psu) sits directly above the NPIW (salinity 34.0–34.1 psu; Kenyon, 1978). Thus along the eastern continental boundary, these features are most easily identified by their density rather than as distinct salinity minima relative to the surrounding waters. However, their characteristic salinity is evident when viewed

Present address: Lamont Doherty Earth Observatory, Palisades, NY 10964, USA.

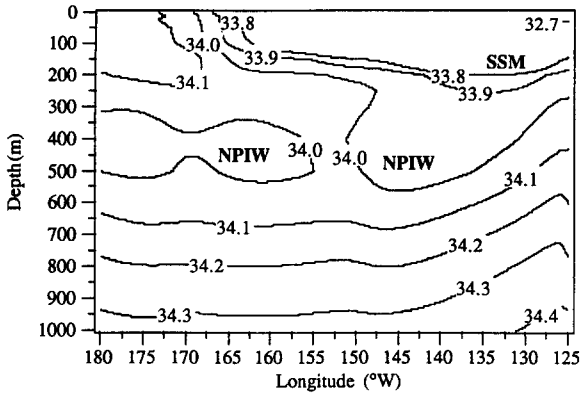

FIG. 1. Winter seasonal (FMA) salinity along 42°N from Levitus (1982). SSM denotes the Shallow Salinity Minimum (32.7–33.9 psu), while NPIW denotes the North Pacific Intermediate Water (34.0–34.1 psu). The MOCNESS plankton tows in this study were collected between 125°W and 132°W.

in meridional salinity sections from Levitus (1982) (Fig. 1) or hydrographic datasets such as that of Kenyon (1978).

The SSM forms in a broad region north of 35°N and generally west of 145°W, then spreads east and south along isopycnal surfaces (Reid, 1973; Talley, 1985). These waters are relatively cold and fresh, as they subduct below the warmer, more saline (but less dense) waters of the California Current and subtropical gyre.

The NPIW at σ_θ = 26.8 does not outcrop in the North Pacific, except perhaps occasionally in the Sea of Okhotsk (Talley, 1991). NPIW appears to form as the result of the mixing of waters from the Oyashio and Kuroshio currents with water from the Sea of Okhotsk in the western Pacific mixed water region (Talley, 1991, 1993). Qiu (1995) demonstrated that the NPIW salinity minimum is concentrated on the σ_θ 26.8 isopycnal because this is the least dense surface which does not outcrop during the winter. Once formed, the low salinity waters of the NPIW spread out along σ_θ 26.8, flow north and east into the Gulf of Alaska, and eventually southward into the California Current. Oxygen and tritium concentrations indicate that the properties of the NPIW are partially reset in the Alaskan Gyre. Van Scoy et al. (1991) and Van Scoy and Druffel (1993) argue some winter outcropping of the NPIW must occur in the Gulf of Alaska, although Talley (1993) attributes the oxygen and tritium changes to diapycnal mixing.

3. METHODS

3.1. Plankton Tow Distributions and Hydrographic Measurements

These study sites are part of the Multitracers program, a study of the California Current System. The MOCNESS plankton tow samples were collected during September 17–30, 1990 during cruise W9009A of the R/V *Wecoma* at four sites 121, 220, 289, and 572 km offshore, roughly at 42°N. All of the tows were located west of the shelf break, which occurs at ≈95 km offshore. In order of increasing distance offshore, they were collected in waters of 2800, 2500, 3000, and 3700 m depth. Methods for plankton tow sample preparation and calculations of precision are in Ortiz et al. (1995). Standing stocks reported here are accurate to ±20% due to the sum of towing, sample splitting, and counting errors.

Temperature and salinity were measured by CTD and used to calculate σ_θ, the potential density of a water parcel. Light transmission at 670 nm wavelength, measured with a SeaTech™ transmissometer, is presented as the particle attenuation coefficient (C_p), a derived quantity which is linearly proportional to concentration of small (<20 μm) particles in the water column (Zaneveld et al., 1979; Pak et al., 1988). C_p in this area is also linearly related to large (>63 μm) particle concentrations (Ortiz et al., 1995). The hydrographic station locations are listed in Table 1.

3.2. Planktonic Foraminiferal $\delta^{18}O_s$ and $\delta^{13}C_s$

Micro-sample isotopic measurement of foraminiferal shell $\delta^{18}O_s$ and $\delta^{13}C_s$, and carbon isotopic measurements of ΣCO2 in the water column ($\delta^{13}C_w$), were made at Oregon State University using a Finnigan/MAT-251 mass-spectrometer. This instrument is equipped with an online Autoprep Systems automated carbonate sample preparation device for the foraminferal samples, and an online tube-cracker use to analyze gas extracted from water samples. Isotopic results are presented in permil (‰) using the standard isotopic delta notation (δ) relative to the Pee Dee Belemnite (PDB) scale. Calibration to PDB was done through the NBS-19 and NBS-20 standards made available by the U.S. National Institute of Standards and Technology.

Typical precision of isotopic measurements of calcite at the OSU laboratory are ±0.06‰ for $\delta^{18}O$ and ±0.03‰ for $\delta^{13}C$. In the present study, isotopic measurements were conducted on smaller sample sizes (5–50 μg calcite) than typical microfossil carbonate analyses (>50 μg calcite), which decreased machine precision somewhat relative to larger size runs. To enhance machine sensitivity and precision for very small samples, (1) the source current was increased from 1.3–1.5 mA, (2) reference gas pressure was decreased to maintain proper adjustment between the sample and reference inlets at low pressures, and (3) vacuum pumping was increased to 30 min between sample runs. Resulting external precision for $\delta^{18}O$ and $\delta^{13}C$ measured on micro-samples of calcite standards ranging in mass from 5–50 μg was ±0.2‰ and ±0.1‰, respectively.

We chose to analyze small samples to assess intraspecific isotopic variation and because the deep-dwelling species were rare in our plankton tows relative to shallow-dwelling species. Running small numbers of individuals allows us to better assess the natural isotopic variability exhibited by each species. Individual shells may exhibit variable disequilibrium effects or calcify over a range of depths. Generally two to ten shells were grouped in each isotopic analysis. For *G. scitula,* shells from the 150–212, 212–250, and 250–300 μm size fractions were analyzed separately. For *G. hexagona* and *G. calida,* individuals in the 125–150, 150–212, 250–300, and 300–355 μm size fractions were analyzed. For left-coiling *N. pachyderma,* (the smallest and rarest of the four species) individuals in the 125–212 μm size fraction were run.

Isotopic analysis of *G. scitula* were conducted on shells collected from the 200–400 m deep sample at each of the four tow sites. Isotopic measurements for the three remaining species were conducted only at the location of the maximum species occurrence, due to limited sample availability. These samples were 400–600 m at the 572 km site for *G. hexagona* and *G. calida,* and 200–400 m and 400–600 m at the 121 km site for left-coiling *N. pachyderma.*

3.3. Water Column $\delta^{18}O_c$ and $\delta^{13}C_c$

To assess foraminiferal calcification depth ranges we predicted the oxygen isotopic composition of inorganic calcite in equilibrium with the water column ($\delta^{18}O_c$), using temperatures and salinities

Table 1

W9009a deep CTD stations.

CTD Station	Depth Range (m)	Latitude (°N)	Longitude (°W)	km from Coast
2	1-2751	42.063	125.905	141
5	3-2652	42.375	126.375	184
6	4-1502	42.082	126.001	149
7	2-2952	42.080	126.997	231
8	0-2751	42.188	127.615	282
14	0-3400	41.592	131.982	646
17	2-2502	41.666	131.233	583
18	0-2951	41.751	130.002	481
19	1-1500	41.832	128.964	394
20	2-1500	41.831	128.200	331
23	3-1002	42.084	125.365	97

obtained from concurrent CTD casts. Salinity was converted to water column oxygen isotopic composition ($\delta^{18}O_w$, in ‰ SMOW) using the Northeast Pacific relationship of Zahn et al. (1991):

$$\delta^{18}O_w = 0.405\ (\text{Salinity}) - 14.01‰. \quad (1)$$

Although direct measurements of $\delta^{18}O_w$ were not conducted as part of this study, the data for Eqn. 1 were obtained from California Current and Northeast Pacific environments similar to those studied here. Values of $\delta^{18}O_c$ were predicted by inverting the paleo-temperature equation of Epstein et al. (1953).

To assess the depth of calcification independently of the tow collection depth, we assume initially that the four species calcified in oxygen isotopic equilibrium with respect to the water column. The is a standard procedure used in many studies, such as Williams et al. (1981), Deuser (1987), and Ravelo and Fairbanks (1992). We relax this constraint later when we consider possible kinetic fractionations. Calcification depth ranges for each species are then obtained by comparison of the mean and standard deviation of measured $\delta^{18}O_s$ to predicted $\delta^{18}O_c$ for the corresponding tow site.

Measurements of water column nutrients (nitrate, phosphate, and silicate) and the carbon isotopic composition of dissolved inorganic carbon ($\delta^{13}C_w$) were made on water samples collected during September 1991 along the same transect as the September 1990 tow sites. Water samples come from CTD casts using 5 L Niskin bottles. Here we report on the nitrate data only. A more detailed analysis of the nutrient data can be found in Ortiz et al. (1996). Samples for nutrients were stored in acid washed 125 cc polyethylene bottles that were rinsed first with sample water. Frozen samples were thawed overnight prior to analysis on an Alpkem RFA autoanalyzer with standard wet chemistry techniques (Gordon et al., 1994). NO_3 concentrations reported here are accurate to 0.8% based on triplicate analysis of surface samples.

Water samples for carbon isotopic analysis were stored in 50 cc, brown reagent grade, pre-baked septum-sealed vials, that were poisoned immediately after filling with mercuric chloride ($HgCl_4$). They were stored under refrigeration in the dark and returned to the OSU laboratory by surface freight immediately after the cruise. In the OSU laboratory, water samples were analyzed using a procedure similar to that of Kroopnick (1974). 20 cc of each water sample was injected into a glass stripping line and acidified with 95% H_3PO_4. ΣCO_2 was evolved as CO_2 gas by stripping with high-purity He flowing through a glass frit. Water vapor and trace volatiles were condensed on a three-loop glass trap filled with clean 2-mm glass balls (to maximize surface area). CO_2 was condensed on a one-loop cold trap containing similar glass balls at liquid nitrogen temperatures. Following stripping and trapping, the He flow was turned off, the CO_2 trap and an additional cold finger was evacuated, isolated, and warmed, and the clean CO_2 was transferred to a 6-mm glass cold finger using liquid nitrogen. The 6-mm glass finger was then torch sealed, and the isolated CO_2 gas sample was transferred to the Oregon State University Finnigan/MAT-251 mass-spectrometer using a multiport/tube cracker system. External precision for the $\delta^{13}C_w$ measurements based on replicate CO_2 gas samples extracted from an internal laboratory water standard following these methods was ±0.04‰.

We compare the carbon isotopic composition of the foraminiferal shells ($\delta^{13}C_s$) to the predicted carbon isotopic composition of inorganic calcite in equilibrium with the dissolved inorganic carbon pool ($\delta^{13}C_c$). Romanek et al. (1992) demonstrated that $\delta^{13}C_c$ is enriched relative to $\delta^{13}C_w$ by 1‰ (within experimental errors of ±0.2‰):

$$\delta^{13}C_c = \delta^{13}C_w + 1.0‰. \quad (2)$$

We compare shell composition, $\delta^{13}C_s$, to $\delta^{13}C_c$ to estimate each species' apparent carbon isotopic disequilibrium. This method yields upper limits on the true $\delta^{13}C$ disequilibrium (thus the term apparent) because at this stage we assume $\delta^{18}O$ equilibrium. Deviations from $\delta^{18}O$ equilibrium that covary with $\delta^{13}C$ disequilibrium would be expressed as an increase in the apparent $\delta^{13}C$ disequilibrium. While this approach introduces some error, numerous studies demonstrate that planktonic foraminifera calcify much closer to $\delta^{18}O$ equilibrium than $\delta^{13}C$ equilibrium (e.g., Erez and Luz, 1983; Deuser, 1987). We assess the magnitude of this error by relaxing the constraint of oxygen isotopic equilibrium later in the paper.

4. RESULTS

4.1. The Local Relationship between Nutrients and $\delta^{13}C_w$

Oceanic $\delta^{13}C_w$ varies inversely with nutrient concentrations due to the concurrent uptake of nutrients and preferential uptake of ^{12}C (relative to ^{13}C) during photosynthesis. The slope of the relationship between phosphate (PO_4) and $\delta^{13}C_w$ depends on the average fractionation of $\delta^{13}C$ during photosynthesis (about −20‰). Given the C:P Redfield ratio for marine organic matter (105), and the mean ocean inorganic carbon concentration (2250 μmol/kg) (Broecker and Peng, 1982), the predicted slope of $\delta^{13}C_w$:PO_4 is −0.93‰/μmol/kg (Broecker and Peng, 1982). This can be scaled relative to nitrogen using the N:P Redfield ratio (16), yielding a predicted $\delta^{13}C_w$:PO_4 slope of −0.06‰/μmol/kg.

At the Multitracers study sites, the direct measurements of $\delta^{13}C_w$ and $[NO_3^-]$ collected in September 1991 are well correlated (Fig. 2, Table 2). However, surface $\delta^{13}C_w$ values (0–200 m) are offset from deeper values (200–2500 m). Measured $\delta^{13}C_w$ correlates better to $[NO_3^-]$ than $[PO_4^{3-}]$ at these sites because residual $[PO_4^{3-}]$ remains in the water column after $[NO_3^-]$ has been stripped to limiting levels by phytoplankton growth (Ortiz et al., 1996). We use shallow and deep relationships obtained from the September 1991 Multitracers $\delta^{13}C_w$ and $[NO_3^-]$ data to determine water column $\delta^{13}C_w$ for the September 1990 tows based on concurrent $[NO_3^-]$ measurements. The relationship for the shallow data (0–200 m) is

$$\delta^{13}C_w = -0.06\ [NO_3^-] + 1.6. \quad (3a)$$

In contrast, measurements from >200 m follow a considerably smaller slope:

$$\delta^{13}C_w = -0.02\ [NO_3^-] + 0.6. \quad (3b)$$

The RMS errors of individual analyses associated with these regressions are similar, ±0.12‰ (n = 28) for the shallow

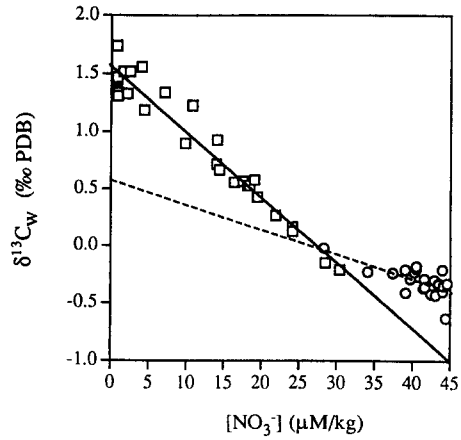

FIG. 2. Relationships between $\delta^{13}C_w$ and $[NO_3^-]$ at 42°N. Shallow waters (<200 m, squares) follow $\delta^{13}C_w = -0.06\ [NO_3^-] + 1.6$ (r^2 = 0.95). Deep waters (>200 m, circles) follow $\delta^{13}C_w = -0.02\ [NO_3^-] + 0.6$ (r^2 = 0.45). Surface to deep offset in $\delta^{13}C$ arises from anthropogenic invasion along isopycnal surfaces during winter ventilation as discussed in the text.

Table 2

Dissolved inorganic carbon $\delta^{13}C$ and $[NO_3^-]$ during September, 1991 at four sites along the Multitracers transect.

Site	Depth (m)	$\delta^{13}C$ (‰ PDB)	$[NO_3^-]$[a] ($\mu M\ kg^{-1}$)	Site	Depth (m)	$\delta^{13}C$ (‰ PDB)	$[NO_3^-]$[a] ($\mu M\ kg^{-1}$)
45 km[b]	0	1.52	1.61	289 km[c]	0	1.52	2.48
	10	1.33	2.14		10	1.56	4.00
	20	1.34	7.07		75	0.72	13.98
	32	1.23	10.78		100	0.57	17.54
	50	0.93	14.06		200	-0.15	28.48
	75	0.58	19.06		400	-0.41	39.11
	100	0.17	24.12		500	-0.36	41.59
					600	-0.30	42.90
121 km[c]	0	0.67	14.36		800	-0.40	44.01
	20	0.56	16.37		1000	-0.63	44.40
	40	0.53	18.42		1500	-0.21	43.94
	50	0.43	19.45		2000	-0.29	41.55
	75	0.27	21.93		2500	-0.20	40.52
	75	0.27	21.93		2500	-0.18	40.52
	100	0.13	24.18				
	200	-0.21	30.35	572 km[c]	0	1.74	0.74
	300	-0.23	34.11		20	1.45	0.76
	400	-0.24	37.42		50	1.47	0.80
	500	-0.29	39.72		95	1.34	0.84
	600	-0.37	41.45		100	1.31	0.85
	1000	-0.43	43.06		120	1.19	4.39
	1500	-0.42	42.46		150	0.90	9.83
					200	0.53	18.10
					300	-0.02	28.30
					500	-0.21	39.06
					800	-0.35	44.10
					1000	-0.33	44.62
					1500	-0.33	43.48
					1500	-0.34	43.48
					2000	-0.23	40.26

[a]Sampling location: 42.105°N, 125.837°W.
[b]Nitrate bottle measurements from the same CTD cast were interpolated to the depths of the $\delta^{13}C$ bottle measuremts.
[c]Identical depths at the same site indicate duplicate $\delta^{13}C$ measurements, the same nitrate measurement is listed for each $\delta^{13}C$ replicate.

(<200 m) samples and ±0.09‰ (n = 22) for the deep (>200 m) samples. The inflection point in this relationship occurs at about 200 m (σ_θ = 26.5), i.e., near the limit of well-ventilated waters (Fig. 2). We infer that well-ventilated shallow waters are offset in $\delta^{13}C_w$ relative to deeper waters by -0.6 ± 0.2‰, due to input of ^{13}C-depleted anthropogenic CO_2. The low slope of the $\delta^{13}C_w$:NO_3 below the 26.5 isopycnal reflects diffusive mixing of recently ventilated waters with poorly-ventilated subsurface waters (Ortiz et al., 1996).

4.2. Water Mass Properties along Isopycnal Surfaces

Associated with southward flow and upwelling in the California Current, isopycnal surfaces are shallowest near the coast, and increase in depth offshore (Fig. 3a). Waters equivalent in density to the SSM (σ_θ 25.1–26.7 kg/m^3) range in temperature from 7–10°C (Fig. 3b) and in salinity from 32.8–33.9 psu (Fig. 3c). NPIW (σ_θ 26.7–26.9 kg/m^3) is less variable, with temperatures of 5.9–6.1°C, and salinities of 33.9–34.1 psu. These ranges are consistent with the temperature and salinity range of the SSM and the NPIW measured elsewhere in the North Pacific (Kenyon, 1978; Yuan and Talley, 1992).

Measurements of C_p within the SSM decrease from 0.10 m^{-1} at the base of the thermocline, to <0.05 m^{-1} offshore and with increasing depth (Fig. 3d). Values of C_p in the NPIW are less variable, ranging from 0.03–0.05 m^{-1}. These C_p values indicate a greater concentration of small particles in the SSM than in the NPIW.

Temperature and salinity across the transect produce estimates of $\delta^{18}O_e$ that are relatively constant along isopycnal surfaces (Fig. 3e). Estimates of $\delta^{18}O_e$ range from 0.5–2.0‰ PDB consistent with its broadly defined densities. The $\delta^{18}O_e$ of NPIW are more narrowly defined, from 2.0 and 2.5‰ PDB.

4.3. Species Distribution Patterns

In our plankton tows, depths of about 200 m ($\sigma_\theta \approx 26.5$) coincide with a transition in foraminiferal faunas, with high standing stocks dominated by shallow-dwelling species above and low standing stocks with potentially deep-dwelling species below. Shallow dwelling species are discussed in Ortiz et al. (1995). Here we investigate the four species observed at greater depths: *G. scitula, G. hexagona, G. calida,* and left-coiling *N. pachyderma.* Algal symbionts have not been reported in any of these species, although data to support this statement is rare for all but left-coiling *N. pachyderma* (Hemleben et al., 1988). We define these species as potentially deep dwelling because they were collected at depths >200 m and contained obvious protoplasm in their shells. Although some shallow dwelling species were also found at similar depths, their shells generally lacked protoplasm below 200 m, and thus represented a settling flux of dead shells.

For each MOCNESS plankton tow sample, Table 3 lists estimates of the volume of water filtered, environmental variables averaged at tow resolution, and foraminiferal standing stocks. *G. scitula* was the most abundant of the four potentially deep-dwelling species. It reached standing stocks of 1.5 shells/m^3. *G. hexagona* and *G. calida* had maximum standing stocks of 0.5 shells/m^3. Left-coiling *N. pachyderma* was more rare, with a maximum of only 0.25 shells/m^3.

When plotted on isopycnal surfaces, the species standing stock distributions fall into two groups. The first group is composed of *G. scitula* and *G. hexagona* (Fig. 4). *G. scitula* was common at all of the sites across the transect, but especially at the site 121 km offshore. With the exception of an isolated occurrence in the surface waters 121 km offshore, *G. scitula* was most abundant within the density range of the SSM or at slightly greater density; i.e., between σ_θ 26.4 and 26.8 at the sites 121, 289, and 572 km offshore, and between σ_θ 25.5 and 25.9 at the site 220 km offshore. *G. hexagona* decreased in abundance toward the coast and was most common between σ_θ 26.8 and 27.2 at all four of the tow sites; i.e., along an isopycnal surface consistent with or of slightly greater density than NPIW.

The second group of species was composed of *G. calida* and left-coiling *N. pachyderma* (Fig. 5). *G. calida* was found in waters of σ_θ <25.4 at the sites 280 and 572 km offshore. It was also found between σ_θ 26.2 and 27.3, at this density horizon it decreased in abundance toward the coast. Left-coiling *N. pachyderma* generally decreased in abundance away from the coast and was not closely associated with any particular isopycnal surface.

4.4. Isotopic Results

The $\delta^{18}O_s$ of *G. scitula* collected from the water column between 200 and 400 m (σ_θ 26.5–26.7), did not vary sys-

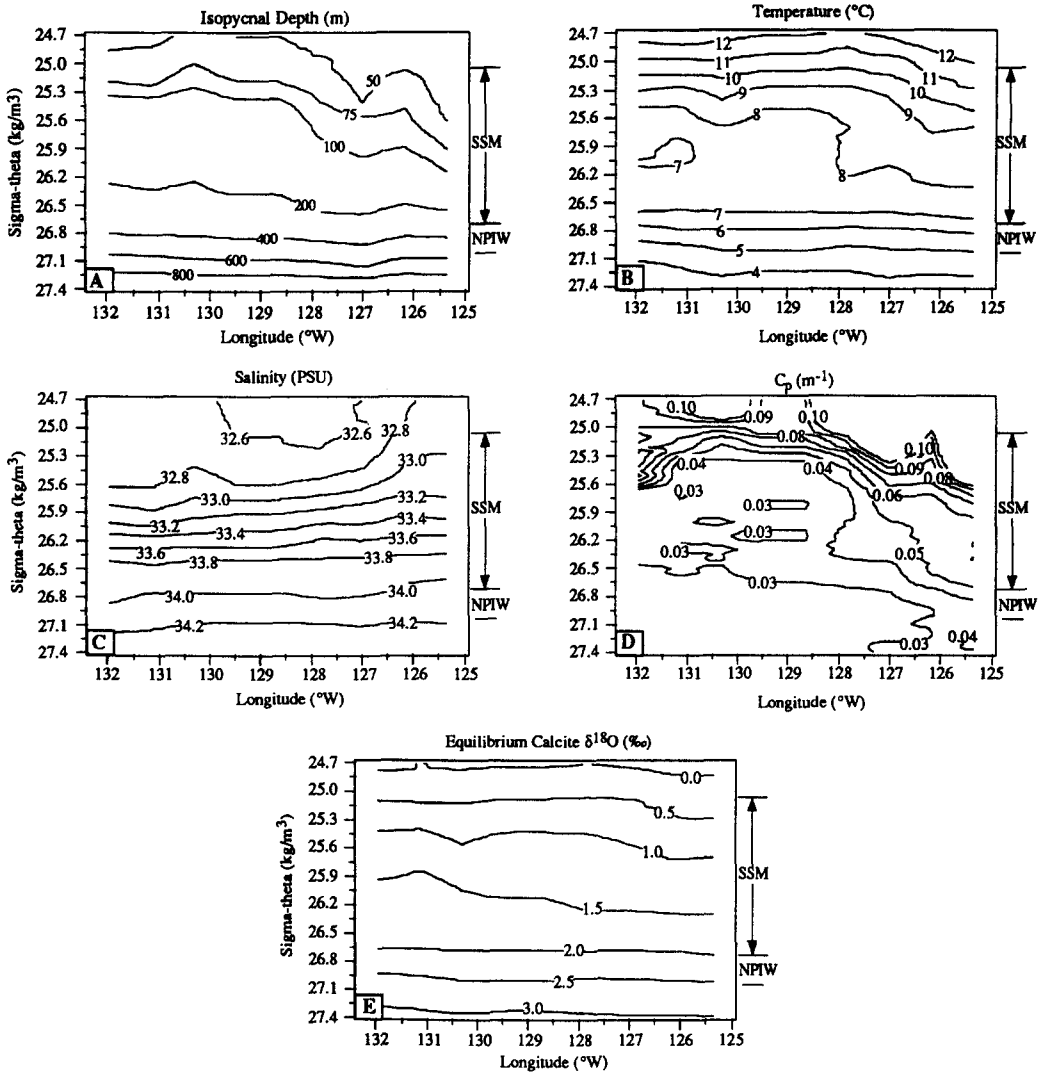

FIG. 3. Deep hydrography on isopycnal surfaces along the Multitracers transect at 42°N. (a) isopycnal depth (in m), (b) temperature (in °C), (c) salinity in psu, (d) transmissometer particle attenuation (C_p, in m^{-1}), and (e) equilibrium calcite $\delta^{18}O$ calculated using methods described in the text. The plots are based on subthermocline data from the CTD stations listed in Table 1. SSM and NPIW mark the properties of these water masses based on their isopycnal range.

tematically with shell size or location (Fig. 6, Table 4). The mean $\delta^{18}O_s$ value, 1.7 ± 0.2‰ PDB (n = 10), was within the range of values predicted for the SSM waters (Fig. 6), and consistent with $\delta^{18}O_e$ from 150–290 m where σ_θ ranges from 26.2–26.7 (Table 5, Fig. 7a). The variability for $\delta^{18}O_s$ is close to the external analytical precision for small size samples, suggesting that much of the measured $\delta^{18}O_s$ variance could be random.

The mean $\delta^{18}O_s$ of *G. hexagona* at the site 572 km offshore is 2.1 ± 0.1‰ PDB (Table 5). This is within the range of $\delta^{18}O_e$ values found within NPIW (Fig. 6), and consistent with equilibrium calcification at depths of 330–390 m (Fig. 7b) or σ_θ 26.7–26.8. Values of $\delta^{18}O_s$ varied little in *G. hexagona* as a function of shell mass (Fig. 6, Table 4).

Left-coiling *N. pachyderma* and *G. calida* have $\delta^{18}O_s$ values much lower than *G. scitula* and *G. hexagona* (Tables 4, 5), similar to $\delta^{18}O_e$ from depths much shallower than those of the SSM or NPIW (Figs. 6, 7). The observed $\delta^{18}O$ values suggest that at the 121 km site left-coiling *N. pachyderma* calcified near the base of the mixed layer (5–35 m) in waters of σ_θ 23.3–24.3. The small sample size (n = 2) and large size fraction for left-coiling *N. pachyderma* prevents us from fully assessing size dependent variations in this species. Variations in $\delta^{18}O_s$ from *G. calida* were similar to those of left coiling *N. pachyderma* (Fig. 6). At the site 572 km offshore, the $\delta^{18}O_s$ of *G. calida* is consistent with equilibrium calcification at depths of 35–55 m (Fig. 7d), or σ_θ 24.3–24.9, which is shallower and less dense than either SSM or NPIW.

In contrast to $\delta^{18}O$ measurements that appear to record equilibrium or near-equilibrium calcification, $\delta^{13}C$ measurements require disequilibrium. $\delta^{13}C$ in three of the species clearly varies as a function of shell mass (Fig. 6). Average $\delta^{13}C$ values of each species plotted in Fig. 6 is lower than

Table 3

MOCNESS plankton tow environmental and foraminiferal data for the potentially deep dwelling species (>125 μm). (Values of Zero omitted for clarity)

Tow site and date	Depth Range (m)	Density Range (kg m^{-3})	Volume Filtered (m^3)	Mean Temp (°C)	Mean Salt (psu)	Mean Density (kg m^{-3})	Mean Cp (m^{-1})	Mean Pdv (ml m^{-3})	*G. scitula* (m^{-3})	*G. hexagona* (m^{-3})	*G. calida* (m^{-3})	Left coiling *N. pachyderma* (m^{-3})
121 km	0-30	24.2 - 24.5	33	14.8	32.8	24.3	0.307	8.5	0.12			0.12
42.060 °N	30-70	24.5 - 25.6	39	10.9	33.0	25.2	0.119	2.3				
125.665 °W	70-100	25.6 - 26.0	114	8.9	33.3	25.8	0.061	0.4	0.07			0.07
9/21/90	100-200	26.0 - 26.5	147	8.0	33.8	26.3	0.054	0.5	0.30			0.05
	200-400	26.5 - 26.8	342	6.7	34.0	26.7	0.042	0.6	1.30			0.07
	400-600	26.8 - 27.1	154	5.2	34.1	27.0	0.030	0.4	0.65	0.05		0.24
	600-800	27.1 - 27.2	134	4.4	34.3	27.2	0.031	0.3	0.24		0.06	0.18
220 km	0-30	23.8 - 23.8	34	16.3	32.6	23.8	0.230	6.3				0.12
42.167 °N	30-70	23.8 - 25.5	20	12.2	32.9	24.9	0.128	3.3				
126.858 °W	70-100	25.5 - 25.9	19	8.9	33.2	25.7	0.058	0.8	0.63			0.21
9/28/90	100-200	25.9 - 26.5	113	8.1	33.8	26.3	0.064	0.3	0.14			0.04
	200-400	26.5 - 26.8	293	6.6	34.0	26.7	0.042	0.4	0.37	0.03		0.06
	400-600	26.8 - 27.1	257	5.2	34.1	27.0	0.029	0.4	0.34	0.03	0.02	
	600-800	27.1 - 27.2	268	4.4	34.3	27.2	0.030	0.2	0.45	0.10	0.07	
289 km	0-60	23.0 - 25.2	57	14.0	32.4	24.1	0.186	5.3			0.35	
42.169 °N	60-100	25.2 - 26.0	40	8.4	32.8	25.5	0.054	1.1				
127.694 °W	100-200	26.0 - 26.6	99	7.7	33.8	26.4	0.044	0.5	0.08			0.04
9/23/90	200-400	26.6 - 26.9	159	6.2	34.0	26.7	0.031	0.7	0.28		0.03	
	400-600	26.9 - 27.1	264	4.8	34.1	27.0	0.024	0.5	0.09		0.03	
	600-800	27.1 - 27.3	329	4.3	34.3	27.2	0.027	0.2	0.01	0.01		0.01
572 km	0-30	23.3 - 24.1	46	17.9	32.6	23.5	0.070	1.1				0.09
41.493 °N	30-70	24.1 - 25.2	72	11.9	32.7	24.8	0.084	1.7			0.11	0.06
131.070 °W	70-100	25.2 - 25.3	32	8.9	32.6	25.3	0.055	1.1			0.12	
9/26/90	100-200	25.3 - 26.3	125	7.5	33.0	25.8	0.031	0.5	0.45			0.03
	200-400	26.3 - 26.8	229	6.6	33.9	26.6	0.028	0.3	0.62	0.05	0.15	
	400-600	26.8 - 27.0	458	5.0	34.1	26.9	0.024	0.2	0.06	0.47	0.38	0.02
	600-800	27.0 - 27.2	258	4.2	34.2	27.1	0.023	0.2	0.68	0.26	0.28	0.02

predictions of equilibrium with NPIW or any water mass of the upper 1000 m of the water column, in contrast with their collection depths. Using the calcification depths estimated from $\delta^{18}O$, we explore the magnitude of the apparent carbon isotopic disequilibrium for each species, and seek a common cause for its occurrence.

The mean $\delta^{13}C$ value for *G. scitula* was $-0.1 \pm 0.2‰$ PDB ($n = 10$), lower by $1.1 \pm 0.5‰$ than $\delta^{13}C_e$ predicted from its $\delta^{18}O$-derived calcification depth (Fig. 8a). The mean $\delta^{13}C$ value for *G. hexagona* is -0.1 ± 0.1, lower by $1.0 \pm 0.2‰$ than $\delta^{13}C_e$ at this species inferred calcification depth (Fig. 8b). We refer to these offsets from equilibrium as the apparent carbon isotopic disequilibrium.

The apparent carbon isotopic disequilibria in left-coiling *N. pachyderma* and *G. calida* are larger than for the deeper dwelling species. If left-coiling *N. pachyderma* calcified over the depth range 5–35 m, as inferred from $\delta^{18}O$, its $\delta^{13}C$ composition is $2.4 \pm 0.2‰$ lower than $\delta^{13}C_e$ (Fig. 8c). The $\delta^{13}C$ of *G. calida* increased systematically with increasing shell mass, even thought no such trend was evident in its $\delta^{18}O$ (Fig. 6). In comparison to the predicted $\delta^{13}C_e$ for waters from 35–55 m, *G. calida* is lower in $\delta^{13}C$ by $1.9 \pm 0.6‰$ (Fig. 8d).

5. DISCUSSION

5.1. Species Habitats within Water Masses

The plankton tow distributions and isotopic results allow us to distinguish between direct and indirect associations with subsurface water masses for each species studied. The recovery of living foraminifera from subsurface water masses could reflect: (1) sinking of a population from shallower habitats, (2) entrainment into a subsurface water mass where it outcrops in the euphotic zone (source water entrainment), or (3) adaptation to special subsurface conditions.

The sinking hypothesis implies the individuals of a species grew and calcified at shallow depths, then sank with little or no further calcification into subsurface water masses where they were collected by the plankton tows. Left-coiling *N. pachyderma* and *G. calida* fit this hypothesis. The $\delta^{18}O$ data also suggests that they only calcified in shallow waters, then descended to depth. These two species are not found exclusively on subsurface isopycnals (Fig. 5). This suggests that (1) only part of their life cycle is spent in subsurface waters, or (2) their occurrence in the deep samples was the result of a sinking event. Left-coiling *N. pachyderma* and *G. calida* thus appear to live relatively near the surface and record these isotopic conditions rather than intermediate water conditions at these sites.

Source water entrainment implies that a seed population of foraminifera enters a water mass close to its site of formation. The entrained population may reproduce and calcify at depth until it eventually dies out. This mechanism could explain the presence of *G. scitula* in the SSM. The SSM is formed by wintertime subduction of southward flowing low salinity waters below the more saline waters of the subtropical gyre. The source region for the SSM lies between 35–

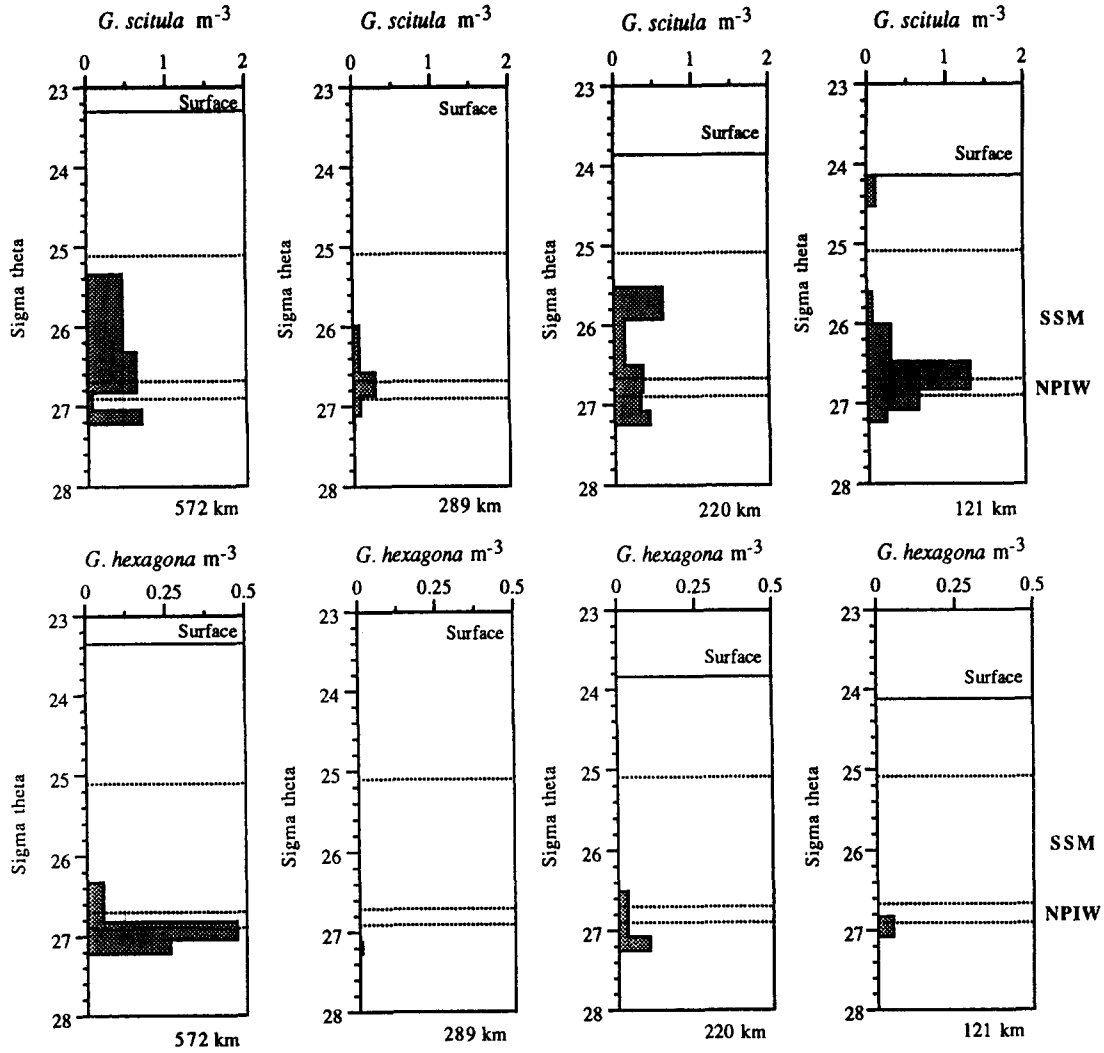

FIG. 4. Standing stock of living *G. scitula* and *G. hexagona* along isopycnal surfaces at the four tow sites 121–572 km offshore. Solid horizontal lines labeled surface mark the shallowest isopycnal at each station. Dashed horizontal lines mark the density range for the SSM (between upper two lines) and NPIW (between the lower two lines).

50°N Latitude, and 140°E–140°W Longitude (Yuan and Talley, 1992). *G. scitula* is a subarctic species found in greater abundance to the north of our sites at locations such as Station P in the Gulf of Alaska (50°N, 145°W; Sautter and Thunell, 1989; Miles, 1973). Near-surface water mass transport from Station P to the Multitracers transect would require on the order of a few months, assuming average current velocities of 10–20 cm s^{-1} (Thompson and Papadakis, 1987). This transit time would enable the production of three to six generations of *G. scitula,* assuming a one month life span (Hemleben et al., 1988).

The adaptation hypothesis implies that a species found at depth is well adapted to its habitat and spends much of its life cycle at depth. This hypothesis seems most applicable to *G. hexagona.* Live individuals of this species were collected below 400 m at each of the four tow sites but were not present in shallow samples. Based on the $\delta^{18}O$ data, this species occupies the deepest habitat of the four species of planktonic foraminifera studied, and has very little $\delta^{18}O$ variation, suggesting calcification exclusively within NPIW. This water mass occupies the shallowest density surface (σ_θ 26.8) that does not outcrop during the wintertime (Qiu, 1995). Thus, it provides a unique, relatively stable environment for organisms adapted to a subsurface existence. NPIW is closest to the surface during the wintertime in the western Pacific mixed water region, and in the Gulf of Alaska. Both areas are north of 40°N. North Pacific plankton tow (Bradshaw, 1959) and sediment studies (Coulbourn et al., 1980), however, demonstrate that *G. hexagona* is most abundant south of 40°N, and is not common where the NPIW is closest to the surface. We conclude that *G. hexagona* is well adapted to life in subsurface waters such as NPIW, that are not rapidly exchanged with surface waters.

G. hexagona may enter NPIW at subtropical latitudes where this waters mass is deep and relatively old. Geostrophic velocities in the core of the NPIW (relative to 2000 m) range from 1–5 cm s^{-1} (Talley et al., 1991; Roemmich and McCallister, 1989; Qiu, 1995). If *G. hexagona* entered

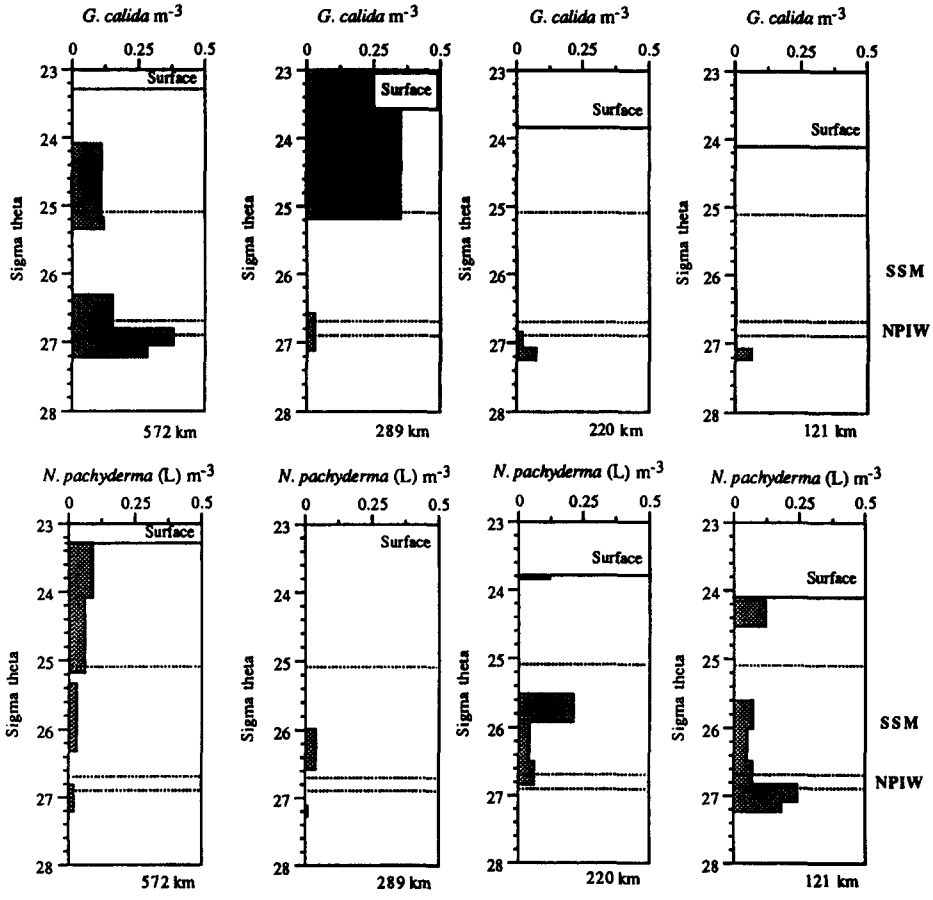

FIG. 5. Standing stock of living *G. calida* and left-coiling *N. pachyderma* along isopycnal surfaces at the four tow sites 121–572 km offshore. Plotting conventions as in Fig. 4.

NPIW in the western Pacific south of 40°N, 5–30 years would elapse before these waters reached the Multitracers transect—too long for an expatriate population with a life span on the order of months (Hemleben et al., 1988) to survive unless it was well adapted to an intermediate water environment.

Summarizing these findings, two of the four species studied seem to be directly associated with the intermediate waters of the northeast Pacific: *G. scitula* with the SSM and *G. hexagona* with the NPIW. *G. scitula,* a subarctic species, is likely to enter the SSM by entrainment during water mass formation and need not be highly adapted to a subsurface habitat, although an adaptation to a subsurface habitat is not entirely ruled out by our data. *G. hexagona,* a subtropical species adapted to a subsurface environment, is likely to be associated with the NPIW (or equivalent water masses that are relatively isolated from the sea surface) during much or all of its life cycle. The remaining species we examined here, left-coiling *N. pachyderma* and *G. calida,* calcified in near surface waters and sank to intermediate waters with little or no additional calcification.

In the next section we explore the apparent carbon isotopic disequilibrium recorded in the shells of these species and attempt to model the signal in all four species as the response to likely environmental forcing functions.

5.2. Apparent Carbon Isotopic Disequilibria

We inferred the apparent calcification depths for the four species based on an assumption of equilibrium calcification with respect to $\delta^{18}O$. Using these depth ranges for each species, we quantify the magnitude of the apparent carbon isotopic disequilibrium ($\Delta\delta^{13}C_{e-s}$), defined as

$$\Delta\delta^{13}C_{e-s} = \delta^{13}C_e - \delta^{13}C_s, \quad (4)$$

where $\delta^{13}C_s$ is the mean carbon isotopic composition of each species shells, and $\delta^{13}C_e$ is the isotopic composition of inorganic calcite formed in equilibrium with $\delta^{13}C_w$, as defined in Eqn. 2. Each of the species studied has a lower $\delta^{13}C_s$ than the predicted equilibrium value, $\delta^{13}C_e$, at its calcification depth. Values of $\Delta\delta^{13}C_{e-s}$ for each species range from 1.0‰ in *G. hexagona* to 2.4‰ in left-coiling *N. pachyderma.* The magnitude of $\Delta\delta^{13}C_{e-s}$ thus decreases with increasing depth of calcification (Fig. 8).

Several depth dependent processes could drive the observed $\Delta\delta^{13}C_{e-s}$ signal. Some possibilities include: (1) changes in the $\delta^{13}C$ of the food source on which the foraminifera feed, (2) changes in isotopic fractionation as a function of temperature, or (3) as a function of food availability. The change in metabolic rate dependent isotopic fractionation postulated in (2) or (3) could result from kinetic fraction,

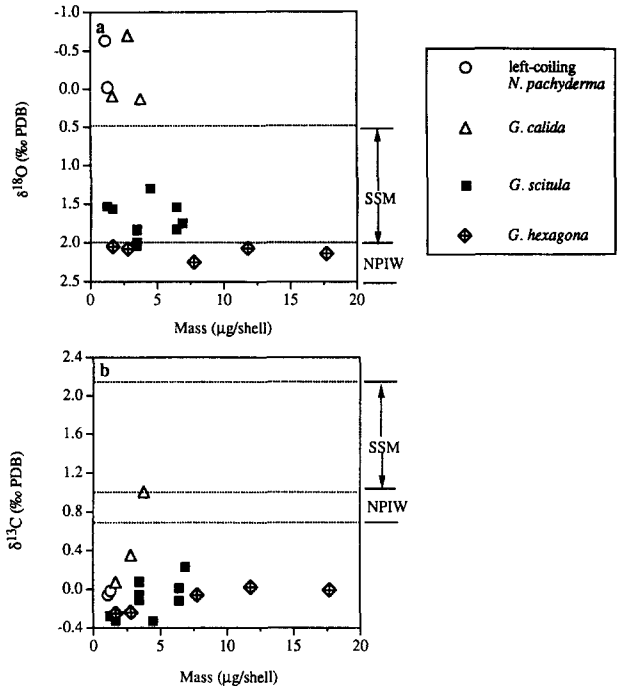

FIG. 6. Oxygen (a) and carbon (b) isotopes for left-coiling *N. pachyderma* (open circle), *G. calida.* (open triangle), *G. scitula* (filled square), and *G. hexagona* (cross within diamond), as a function of average shell mass. SSM and NPIW mark the isotopic ranges of these two water masses for comparison to the foraminiferal measurements.

or from the incorporation of variable amounts of metabolic CO_2 into the shell. These two effects, if operating independently could be distinguished because kinetic fractionation results in a correlated isotopic shift of both $\delta^{18}O$ and $\delta^{13}C$, while the direct effect of metabolic CO_2 incorporation shifts only the $\delta^{13}C$ of the shell (McConnaughey, 1989a,b).

The first process listed above implies metabolic CO_2 of varying isotopic composition is incorporated into the shell during the calcification process, and that deep dwelling foraminifera feed on organisms from a higher trophic level than shallow dwelling foraminifera because of ^{13}C enrichment with increasing trophic level. Body tissue for organisms feeding at progressively higher trophic levels rise in $\delta^{13}C$ by roughly 1‰ per trophic step (DeNiro and Epstein, 1978; Rau et al., 1983).

However, experimental evidence demonstrates the carbon isotopic shift incorporated into the calcareous shells of planktonic foraminifera in response to changes in dietary $\delta^{13}C$ is much smaller than 1‰ for each trophic step. The laboratory study of Spero and Lea (1993) detected no change in the $\delta^{13}C_s$ of the symbiotic foraminifera *O. universa* in response to an 8‰ $\delta^{13}C$ offset in its food. In a second laboratory study, Spero and Lea (1996) observed a −0.54‰ shift in the $\delta^{13}C$ of the asymbiotic species *G. bulloides* in response to a −6.8‰ shift in $\delta^{13}C$ of its diet. Based on these data, the shell $\delta^{13}C$ response of planktonic foraminifers varies from 0–0.08‰ for each 1‰ change in dietary $\delta^{13}C$. Thus for diet to account for the 1.4‰ disequilibrium gradient observed in the asymbiotic foraminifera of the California Current, the deep dwelling species would have to be feeding on a dietary source that was 17–18‰ higher in cellular $\delta^{13}C$ than the shallow dwelling species. This range is not observed in typical marine organic matter. We conclude variations in dietary $\delta^{13}C$ is not the cause of the carbon isotopic disequilibrium observed.

In contrast, both temperature and food directly influence foraminiferal metabolic rate, which should exert an effect on the calcite formation process, and thus vary the magnitude of carbon isotopic fractionation. Under this hypothesis, we construct two models based on simple physiological concepts in an attempt to simulate the carbon isotopic disequilibrium. We begin with a model describing the carbon isotopic disequilibrium solely as a function of temperature, then develop a similar model based solely on food concentration.

Over a small range of values the effect of temperature on a metabolic process typically follows an exponential relationship of the form

$$R_i = R_o Q_{10}^{(T_i - T_o)/10}, \quad (5)$$

where R_i and R_o are metabolic rates measured at two temperatures T_i and T_o (e.g., Schmidt-Nielsen, 1985). The exponential base, referred to as Q_{10}, defines the rate of change of the metabolic process for each 10°C change in temperature. A metabolic rate which doubles over a 10°C temperature increase has $Q_{10} = 2$, one that triples has $Q_{10} = 3$, and so on. The value of Q_{10} is not constant over large temperature ranges and varies when animals are physiologically stressed. Protists typically exhibit Q_{10} values in the range from 1–4 (Bijma et al., 1990; references therein). Working with a variety of planktonic foraminifera over a large range of temperature (10–35°C), Bijma et al. (1990) measured Q_{10} values ranging from 1–9. Near a foraminiferal species' temperature optimum Q_{10} ranged from 2–5. Assuming the isotopic contrast $\Delta\delta^{13}C_{c-s}$ is a proportional to the carbon isotopic fractionation during calcification, we develop a specific function based on Eqn. 5,

$$\Delta\delta^{13}C_i = \Delta\delta^{13}C_o Q_{10}^{(T_i - T_o)/10}, \quad (6)$$

where $\Delta\delta^{13}C_i$ and $\Delta\delta^{13}C_o$ are abbreviated notations for the

Table 4
Oxygen and carbon isotopic composition of the planktonic Foraminifera.

Species	Site	depth range, m	Shell length, µm	Shell mass, µg	δ18O, ‰ PDB	δ13C, ‰ PDB
N. pachyderma (L)	121 km	200-400	177	1.1	-0.63	-0.06
N. pachyderma (L)	121 km	400-600	180	1.3	-0.02	-0.02
G. calida	572 km	400-600	271	1.7	0.09	0.07
G. calida	572 km	400-600	362	2.8	-0.70	0.35
G. calida	572 km	400-600	393	3.8	0.13	1.00
G. scitula	121 km	200-400	203	1.2	1.53	-0.28
G. scitula	121 km	200-400	300	3.4	2.04	0.07
G. scitula	121 km	200-400	290	3.4	1.84	-0.06
G. scitula	121 km	200-400	395	6.4	1.83	-0.12
G. scitula	289 km	200-400	300	3.4	2.00	0.08
G. scitula	572 km	200-400	223	1.6	1.56	-0.33
G. scitula	572 km	200-400	240	3.4	1.83	-0.11
G. scitula	572 km	200-400	295	4.4	1.30	-0.33
G. scitula	572 km	200-400	450	6.9	1.75	0.23
G. scitula	572 km	200-400	345	6.4	1.54	0.01
G. hexagona	572 km	400-600	224	1.7	2.05	-0.25
G. hexagona	572 km	400-600	255	2.8	2.08	-0.24
G. hexagona	572 km	400-600	358	7.8	2.25	-0.06
G. hexagona	572 km	400-600	415	11.8	2.07	0.02
G. hexagona	572 km	400-600	400	17.7	2.14	-0.01

Table 5
Average oxygen and carbon isotopic composition for the four planktonic Foraminiferal species.

Tow site	Species and Number of analysis		Mean $\delta^{18}O$ and STD (‰ PDB)	Mean $\delta^{13}C$ and STD (‰ PDB)	Depth Range[a] (m)	Density Range[b] (kg/m^3)	Mean T and STD[c] (°C)	Mean Cp and STD[d] (m^{-1})	Mean $\Delta\delta^{13}C_{e-s}$ and STD[e] (‰ PDB)
121 km	Left-coiling *N. pachyderma*	(2)	-0.33±0.43	-0.04±0.03	5-35	23.3-24.3	14.5±0.6	0.285±0.047	2.39±0.24
572 km	*G. calida*	(3)	-0.16±0.47	0.47±0.48	35-55	24.3-24.9	12.7±1.0	0.093±0.005	1.85±0.56
121 km	*G. scitula*	(4)	1.81±0.21	-0.10±0.15					
289 km	*G. scitula*	(1)	2.00	0.08					
572 km	*G. scitula*	(5)	1.60±0.21	-0.11±0.24					
Average	*G. scitula*	(10)	1.72±0.23	-0.08±0.19	150-290	26.2-26.7	7.2±0.2	0.039±0.011	1.10±0.48
572 km	*G. hexagona*	(5)	2.14±0.08	-0.11±0.13	330-390	26.7-26.8	6.2±0.1	0.027±0.001	1.00±0.20

[a,b] Calcification depth and density ranges were calculated by comparison of the Foraminiferal shell oxygen isotope values with the $\delta^{18}O$ of calcite in equlibrium with concurrent CTD measured T and S.
[c] The CTD measured temperature over the inferred calcification depth range.
[d] The transmissometer measured particle attenuation coefficient over the inferred calcification depth range.
[e] The apparent carbon disequilibrium is defined as: $\Delta\delta^{13}C_{e-s} = \delta^{13}C_e - \delta^{13}C_s$, where $\delta^{13}C_s$ is the average shell carbon isotope composition, and $\delta^{13}C_e$ is the average equilibrium calcite carbon isotopic composition.

apparent carbon isotopic disequilibrium as defined in Eqn. 4 at two temperatures, T_i and T_o. Using this relationship, a least squares regression determines the $\Delta\delta^{13}C_{e-s}$ and temperature data are best fit by $Q_{10} = 2.75$, yielding an $r^2 = 0.99$ (Fig. 9a). We used the data from *G. hexagona* to specify $T_o = 6.2$°C and $\Delta\delta^{13}C_o = 1.0$‰. The best fit value of Q_{10} is well within the range of typical values observed for protists but may exhibit some bias due to the assumption of oxygen isotopic equilibrium.

The relationship in Eqn. 6 is potentially useful as a paleoceanographic tool. An expression for $\delta^{13}C_e$ based on $\delta^{13}C_s$ and calcification temperature (a specific value of T_i which we denote, T_c) is easily obtained by substituting the right-hand side of Eqn. 6 (with appropriate change of notation) into the left-hand sided of Eqn. 4, then solving for $\delta^{13}C_e$:

$$\delta^{13}C_e = \delta^{13}C_s + \Delta\delta^{13}C_o Q_{10}^{(T_c - T_o)/10}. \quad (7)$$

Note that because Q_{10} is not constant over very broad temperature ranges, it would be dangerous to extrapolate Eqn. 7 beyond the range of its calibration data. Based on the limits of our field data, this expression appears to hold for asymbiotic planktonic foraminifera when T_c ranges from 6–15°C using $Q_{10} = 2.75$, $T_o = 6.2$°C, and $\Delta\delta^{13}C_o = 1$‰ (Fig. 9a). Translation of $\delta^{13}C_e$ to $\delta^{13}C_w$ merely requires the subtraction of 1‰ following Romanek et al. (1992). A

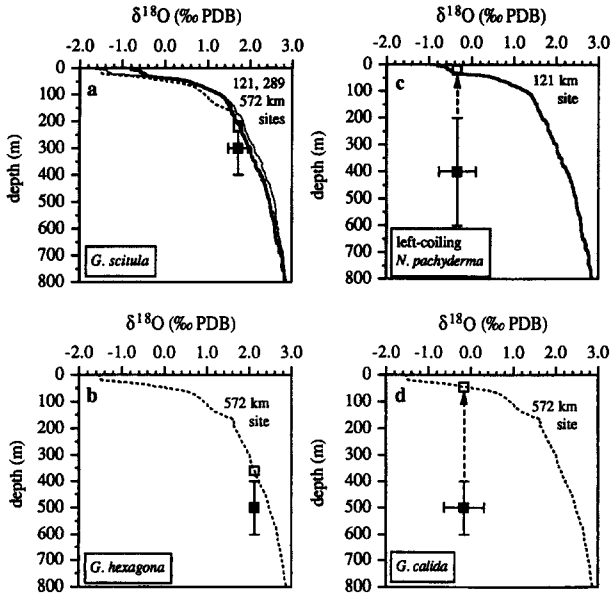

FIG. 7. Average $\delta^{18}O$ as a function of water depth for: (a) *G. scitula*, (b) *G. hexagona*, (c) left-coiling *N. pachyderma*, and (d) *G. calida*. Vertical bars on species data denote tow depth interval. Horizontal bars on the average $\delta^{18}O$ denote the $\delta^{18}O$ standard deviation. Predictions of $\delta^{18}O_e$ at the 121 km site (heavy solid curve), 289 km site (thin solid curve), and 572 km site (dashed curve) are plotted for comparison to the foraminiferal data. Dashed vertical arrows and open squares mark each species' calcification depth inferred from the $\delta^{18}O$ data.

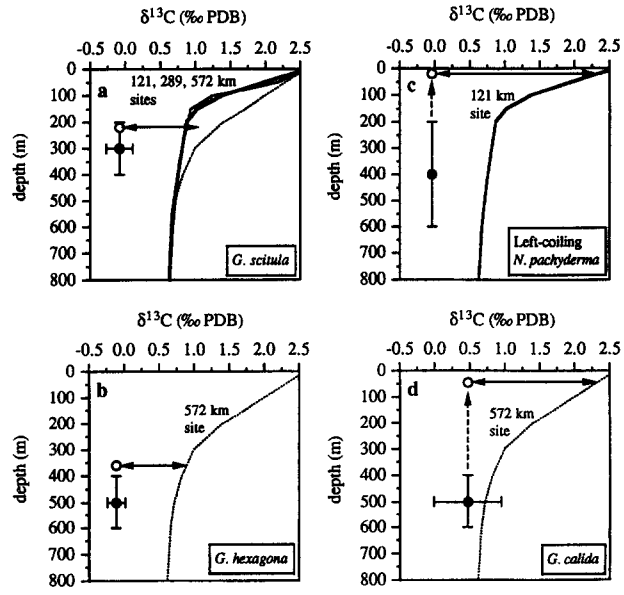

FIG. 8. Carbon isotopes as a function of water depth for: (a) *G. scitula*, (b) *G. hexagona*, (c) left-coiling *N. pachyderma*, and (d) *G. calida*. Plotting conventions as in Fig. 7. Predictions of $\delta^{13}C_e$ at the 121 km site (heavy solid curve), 289 km site (thin solid curve), and 572 km site (dashed curve) are plotted for comparison to the foraminiferal data. Open circles and double headed horizontal arrows yield the species apparent carbon isotopic disequilibria ($\Delta\delta^{13}C_{e-s}$) inferred from the $\delta^{18}O$ calcification depths.

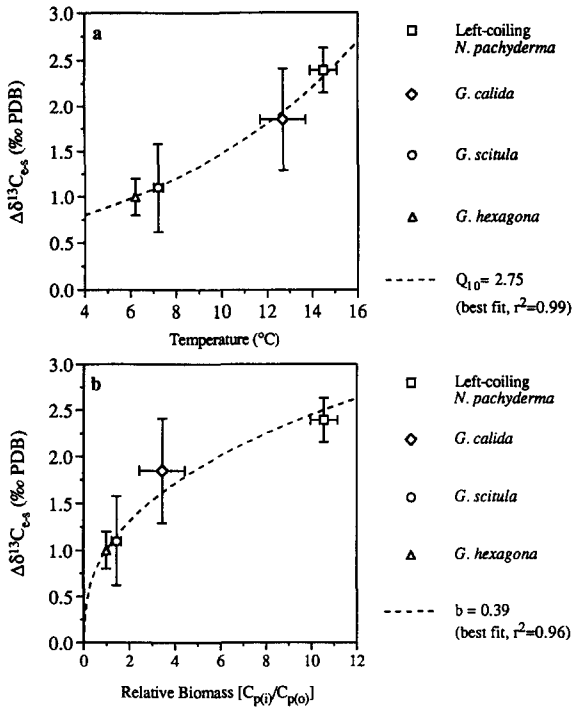

FIG. 9. Apparent carbon isotopic disequilibria ($\Delta\delta^{13}C_{e-s}$) for each species as a function of (a) calcification temperature, and (b) relative biomass based on C_p. Error bars represent standard deviations for carbon isotopes, temperature, and C_p as appropriate.

relationship of this form could be used to determine $\delta^{13}C_e$ and thus $\delta^{13}C_w$ in paleoceanographic applications if T_c can be specified independently.

Temperature is not the only factor that varies with depth at these sites which could cause a change in the foraminiferal metabolic rate. An increase in available food could also drive a change in metabolic rate and thus result in large changes in the carbon isotopic fractionation. Changes in C_p across the transect provide a crude measure of the food available to planktonic foraminifera at the time of collection. While food concentration must affect the metabolic rate of the foraminifera, its relationship to the isotopic composition of their shell is less certain. Spero and Lea (1993) reported no effect on shell $\delta^{13}C$ in symbiotic *O. universa* fed daily and every other day. Because these two feeding regimes may not reflect the full range of natural foraminiferal feeding rates, we attempt to model $\Delta\delta^{13}C$ as a function of the observed food concentration estimated from C_p at our sample locations.

We begin with the observation that a metabolic rate change in response to an increasing biological substrate such as food concentration generally follows a logarithmic relationship (e.g., Schmidt-Nielsen, 1985). This suggests a model of the form

$$R_i = R_o[F_i/F_o]^b. \quad (8)$$

According to this relationship, the initial metabolic rate R_o increases to R_i as determined by the exponent b when the food concentration F_o increases to F_i. Note that when $F_i = F_o$, $R_i = R_o$. To develop a more specific function, we assume once more that the isotopic contrast $\Delta\delta^{13}C_{e-s}$ is proportional to the carbon isotopic fractionation during calcification, and use values of C_p from different depths to obtain Eqn. 9:

$$\Delta\delta^{13}C_i = \Delta\delta^{13}C_o[C_{p(i)}/C_{p(o)}]^b. \quad (9)$$

Here $C_{p(i)}$ and $C_{p(o)}$, which are substituted for F_i and F_o represent the relative change in food as a function of depth. The variables $\Delta\delta^{13}C_i$ and $\Delta\delta^{13}C_o$ are abbreviated notations for the apparent carbon isotopic disequilibrium as defined in Eqn. 4, resulting from the food concentrations defined by $C_{p(i)}$ and $C_{p(o)}$. Once again, we use data from *G. hexagona* and its depth habitat for the initial conditions ($C_{p(o)}$ = 0.027 m^{-1} and $\Delta\delta^{13}C_o$ = 1.0‰). The logarithmic relationship can be solved by least squares regression which yields b = 0.39 with an associated r^2 = 0.96 (Fig. 9b).

As with temperature, it is also possible to derive an expression for $\delta^{13}C_e$ based on $\delta^{13}C_s$ and relative biomass using Eqns. 4 and 9:

$$\delta^{13}C_e = \delta^{13}C_s + \Delta\delta^{13}C_o[C_{p(i)}/C_{p(o)}]^b. \quad (10)$$

Again, we note the danger of extrapolation. This expression should be valid for asymbiotic planktonic foraminifera only when $[C_{p(i)}/C_{p(o)}]$ ranges from 1–12, using b = 0.39, $C_{p(o)}$ = 0.027 m^{-1}, and $\Delta\delta^{13}C_o$ = 1‰.

These modeling exercises demonstrate that variations in either temperature or food concentration may be associated with the depth-related changes in $\Delta\delta^{13}C_{e-s}$, suggesting a link between $\Delta\delta^{13}C_{e-s}$ and variations in metabolic rate. While both models fit variation in $\Delta\delta^{13}C_{e-s}$, the temperature based model has better potential for practical application. It seems plausible that food and temperature should produce additive effects on the magnitude of $\Delta\delta^{13}C_{e-s}$ in the field data. However, our estimate of Q_{10} is typical of protistan values, suggesting that temperature changes may be adequate to describe the depth-related variation in $\Delta\delta^{13}C_{e-s}$.

Laboratory studies of protistan growth rates as a function of food concentration at controlled temperatures estimate that b is ≈0.04 at 12°C, and ranges from 0.2–0.6 at 20°C (Heinbokel, 1978; Sherr et al., 1983; Strom, 1991; Verity, 1991). Our estimate of b = 0.39 is within this range, but rather high considering the low temperatures of our study (6–15°C). We speculate that the large apparent value of b in our model results from the systematic change in prey density as a function of temperature (near surface waters have more biomass).

The data thus seem to imply that temperature has a greater affect on the magnitude of $\Delta\delta^{13}C_{e-s}$ than food concentration. Spero (1988) and Hemleben et al. (1988) demonstrated that calcification in *Orbulina universa* is a discrete process that requires very large energy reserves. A greater lapse of time between chamber formation thus passes in waters with low food concentration than in waters with high food concentration. While the time between calcification events (i.e., chamber formation rate) may be controlled by food concentration and energy storage, the calcification rate, and thus the magnitude of $\Delta\delta^{13}C_{e-s}$ during a chamber formation event may be more sensitive to other factors.

5.3. Evaluating Kinetic Disequilibrium in $\delta^{18}O$

We have so far assumed oxygen isotopic equilibrium. Is it possible there is an oxygen isotopic disequilibrium that we have not accounted for? Perhaps. A kinetic disequilibrium in both the $\delta^{18}O$ and $\delta^{13}C$ of biogenic carbonates may arise from the inorganic dehydration and hydroxylation reactions between CO_2 and HCO_3^- during the calcification process McConnaughey (1989a,b). If CO_2 is the primary substrate for calcification as postulated by McConnaughey (1989a,b), and it is incorporated into the calcite shell faster than it can equilibrate with the ambient water, then disequilibrium in $\delta^{18}O$ and $\delta^{13}C$ should covary. The time for oxygen and carbon isotopic equilibration is on the order of minutes, similar to the time for calcite precipitation in foraminifera. Thus, the extent of disequilibrium may be a function of the organism's calcification rate, which is in turn controlled by cross-membrane flux and adsorption of CO_2 in a solution enriched in Ca^{2+} by ATP-driven $Ca^{2+}/2H^+$ exchange.

The energy intensive, ATP-driven, $Ca^{2+}/2H^+$ pump is likely to be sensitive to the organism's metabolic rate. For example, McConnaughey and Whelan (1996) provides estimates for the activation energy of calcium ATP-ase that range from 50–60 kJ/mol. Using an average estimate of 55 kJ/mol and solving the thermodynamic rate constant equation of Arrehenius at two temperatures separated by 10°C, we can obtain a crude estimate of the Q_{10} temperature dependency of this active transport process. Averaged over the temperature range from 10–20°C, this calculation yields $Q_{10} = 2.2$, which is slightly lower than our estimate of $Q_{10} = 2.75$ given above. One possible explanation for this discrepancy is bias associated with our assumption of oxygen isotopic equilibrium.

If kinetic disequilibrium effects are present in the Multitracers data, their results could be seen graphically in two ways. First, plots of $\delta^{18}O$ or $\delta^{13}C$ as a function of calcification rate would trend away from equilibrium toward lower values with increasing calcification rate. Second, because of a linear correlation between the carbon and oxygen disequilibrium effects, a scatter plot of $\delta^{18}O$ vs. $\delta^{13}C$ will follow a positive slope which trends away from the equilibrium point. As the calcification rate increases, $\delta^{18}O$ and $\delta^{13}C$ become progressively lower, shifting the skeleton's isotopic composition further from equilibrium.

Based on coral data and abiotic laboratory studies, McConnaughey (1989a,b) argued that disequilibrium calcification of this kind occurs in most calcifying organisms, assuming basic calcification methods do not vary greatly with taxonomy. He cited published isotopic data for benthic and planktonic foraminifera as well as several other taxonomic groups to support this statement (e.g., Vergnaud Grazzini, 1976; Vinot-Bertouille and Duplessy, 1973). The slope of the $\delta^{18}O$ to $\delta^{13}C$ disequilibrium relationship appears somewhat variable. McConnaughey (1989a) reported $\delta^{18}O$:$\delta^{13}C$ slopes that ranged from ≈0.3–1.0. Controlled laboratory culture experiments with the asymbiotic foraminifer *G. bulloides* found slopes of 0.32 and 0.37 at 16°C and 22°C (Spero and Lea, 1996). McConnaughey et al. (1996) also suggests a value near 0.33 for the $\delta^{18}O$:$\delta^{13}C$ slope of corals. Reasons for variations in the slope are not well constrained at this time, though ontogenetic effects and environmental factors such as temperature are possible causes. Because some of the CO_2 utilized during the calcification process is of metabolic origin, its isotopic composition may affect the slope. For example, hermatypic corals exhibited steeper slopes than ahermatypic corals, because the presence of photosymbionts shifts the isotopic composition of the carbon pool from which the coral skeleton is built to higher $\delta^{13}C$ values.

Our first test for $\delta^{18}O$ kinetic disequilibrium effects is to plot the isotopic data against shell mass, which we assume is proportional to calcification rate within each species (Fig. 6). A conclusive result would indicate systematic trends in both $\delta^{13}C$ and $\delta^{18}O$ vs. shell mass. While the $\delta^{13}C$ data demonstrates clear trends in three of the four species studied (Fig. 6b), we observed no systematic $\delta^{18}O$ variation within each species as a function of shell mass (within the measurement error of ±0.2‰). Based on the field and laboratory studies noted above, the $\delta^{18}O$ trend could be as small as $^1/_3$ the magnitude of the $\delta^{13}C$ trend. This first test is thus inconclusive, since the smaller $\delta^{18}O$ trend could be obscured by our measurement error of ±0.2‰.

As a second test for kinetic disequilibrium, we plot each species' $\delta^{13}C$ values against its $\delta^{18}O$ values to determine the slope of the data relative to equilibrium points derived from water mass properties at the depth interval from which the shells were collected (Fig. 10). The results suggest that *G. scitula* and *G. hexagona* have $\delta^{18}O$:$\delta^{13}C$ slopes of 0.35 and 0.40, in agreement with the results of Spero and Lea (1996) and McConnaughey et al. (1996). This result implies *G. scitula* and *G. hexagona* have shell $\delta^{18}O$ values lower than $\delta^{18}O_e$ by ≈ −0.4‰. Disequilibrium $\delta^{18}O$ effects of this magnitude would decrease our estimates of $\Delta\delta^{13}C_{e-s}$ for these two species by <0.2‰, which is within the natural variability we report.

For *G. calida* and left coiling *N. pachyderma* our second test generates unrealistically high $\delta^{18}O$:$\delta^{13}C$ slopes of 10.5 and 3.3, respectively (Fig. 10). We infer the artificially large slopes occur due to the settling of these species through the water column without additional calcification. If we use an average $\delta^{18}O$:$\delta^{13}C$ slope of 0.37 determined from the two deeper dwelling species to estimate the equilibrium points for the shallow species, the results suggest that the $\delta^{18}O$ of *G. calida* is lower than equilibrium by ≈ −0.6‰, and the $\delta^{18}O$ of left coiling *N. pachyderma* is lower than equilibrium by ≈ −0.7‰. Disequilibrium $\delta^{18}O$ effects of this magnitude would decrease our estimates of $\Delta\delta^{13}C_{e-s}$ for these two species by −0.3‰ for *G. calida* and by −0.5‰ for left coiling *N. pachyderma.* This result suggests that our initial estimate of $Q_{10} = 2.75$ is slightly exaggerated due to our initial assumption of oxygen isotopic equilibrium, but does not invalidate the concepts behind our model. Correction of the $\Delta\delta^{13}C_{e-s}$ values by −0.3‰ for *G. calida* and by −0.5‰ for left coiling *N. pachyderma* yields a Q_{10} value closer to the thermodynamic estimate of 2.2 (see below).

As a final test for the affect of $\delta^{18}O$ disequilibrium on the Q_{10} model, we apply our model to laboratory measurements of the asymbiotic planktonic foraminifera, *G. bulloides* using isotopic data from Spero and Lea (1996). The data of Spero and Lea (1996) provide a strict test of our model because their foraminifera were cultured under know conditions.

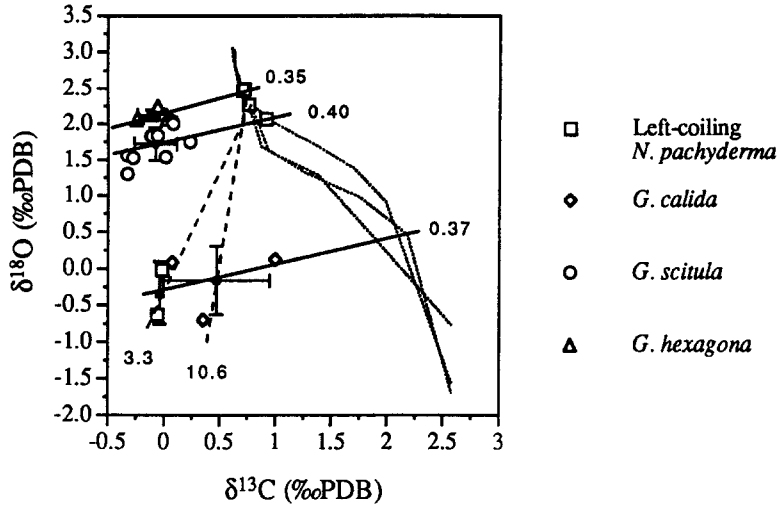

FIG. 10. Carbon isotopes plotted against oxygen isotopes as a test for kinetic isotopic fraction. Thin dashed curves represent the isotopic composition of equilibrium calcite based on water column conditions at the tow sites. The open squares on the thin dashed curves denote potential equilibrium points for each species based on the average isotopic properties of the plankton tow collection interval. *G. hexagona* (cross within diamond) and *G. scitula* (filled square) deviate from equilibrium with $\delta^{18}O$:$\delta^{13}C$ slopes of 0.35 and 0.4, an indication of kinetic isotope fractionation. Data from *G. calida.* (open triangle), and left-coiling *N. pachyderma* (open circle) yield unrealistically large slopes of 10.6 and 3.3, suggesting they could not have calcified at the depth of their collection in the plankton tows. Use of an average slope of 0.37 based on the deep species data provides a realistic estimate of the true equilibrium points for these species.

These authors grew *G. bulloides* under a constant feeding regime at temperatures of 16 ± 0.2°C and 22 ± 0.2°C in water with known $\delta^{13}C_w$ that varied by ±0.2‰. Their results based on amputated, pooled, final chambers are plotted in Fig. 11 along with the Multitracers $\Delta\delta^{13}C$ estimates which have been corrected for oxygen isotopic disequilibrium as described above. The combined datasets are best fit by Eqn. 6 when $Q_{10} = 2.0$, $\Delta\delta^{13}C_o = 1.0$, and $T_c = 6.2$. These results provide strong support for our concept of temperature related carbon isotopic disequilibrium in asymbiotic planktonic foraminifera. The deviation of the estimated $\Delta\delta^{13}C_{e-s}$ for left coiling *N. pachyderma* and *G. calida* which result in our initial over estimate of Q_{10} appear to arise largely from oxygen isotopic disequilibrium as discussed above, with a possible smaller effect due to changes in food concentration with depth.

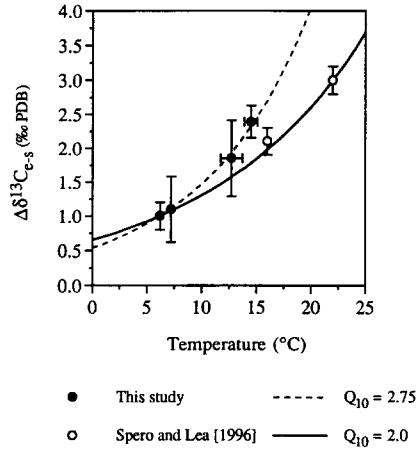

FIG. 11. Comparison of the apparent carbon isotopic disequilibrium estimates for the asymbiotic foraminifera of the California Current (filled circles) with laboratory measurements of actual carbon isotopic disequilibrium for the asymbiotic foraminifera *G. bulloides* (open circles). The data are best fit with $Q_{10} = 2.0$ (solid curve), confirming the presence of a temperature related disequilibrium effect. The deviation of the estimated $\Delta\delta^{13}C_{e-s}$ for left coiling *N. pachyderma* and *G. calida* arises largely from oxygen isotopic disequilibrium, with a smaller effect due to changes in food concentration with depth. Laboratory data from Spero and Lea (1996).

6. CONCLUSIONS

G. scitula and *G. hexagona* reside in, and record the $\delta^{18}O$ of the SSM and NPIW, respectively, with deviations from equilibrium of < -0.4‰. *G. scitula* is likely to enter the SSM from the north through source water entrainment. *G. hexagona* may be adapted to an intermediate water habitat throughout its life span. These findings may be of use in reconstructing the shallow ventilation history of the NE Pacific on geologic timescales. Two other species collected at depth in our samples, left-coiling *N. pachyderma* and *G. calida,* were not exclusively associated with subsurface water masses in the California Current. These species appeared to calcify in the lower mixed layer and upper thermocline at these sites with deviations from $\delta^{18}O$ equilibrium of −0.6‰ for *G. calida* and −0.7‰ for left-coiling *N. pachyderma.* The $\delta^{18}O$ of these two species indicates their occurrence in the deep samples was the result of a settling event. Isotopic disequilibrium appears to influence shell $\delta^{13}C$ significantly in all four of these species.

Shell $\delta^{13}C$ values are ≈2‰ lower than water column equilibrium $\delta^{13}C$ for shallow species, but decrease to 1‰ lower than equilibrium for the deeper dwellers. We propose a phys-

iological model to explain this trend in which either (1) contributions of metabolic CO_2 with low $\delta^{13}C$ or (2) kinetic isotope effects increase as temperature or food supply increase. We speculate that temperature is the stronger control, via its influence on metabolic rate. Our observation of a linkage between isotopic disequilibrium and large-scale environmental variables in the open ocean suggests the possibility that independent knowledge of calcification temperatures (T_c) and/or paleoproductivity will enable the translation of $\delta^{13}C$ measurements from asymbiotic foraminiferal shells into unbiased records of dissolved inorganic carbon $\delta^{13}C$.

Acknowledgments—We thank the captain and crew of R/V *Wecoma,* the Multitracers sediment trap group, and M. Hill and M. Willis for help with the MOCNESS. J. Huyer and B. Smith gave helpful insights on hydrography. We thank P. Wheeler who provided the nitrate data for comparison to the $\delta^{13}C_w$ measurements. The text was improved by comments from: N. Pisias, P. Wheeler, M. Abbott, and P. Froelich. Insightful reviews by C. Charles, H. Spero, and T. McConnaughey improved the manuscript. We thank H. Spero and D. Lea, and T. McConnaughey for the use of data from their unpublished manuscripts. Funding for this project was provided by a NASA Graduate student fellowship to the first author, and by NSF funding to the Multitracers project. Curation of the plankton tow samples at the NORCOR Marine Geological Repository at OSU was provided by a grant from the NSF.

Editorial handling: P. N. Froelich

REFERENCES

Bijma J., Faber W. W., Jr., and Hemleben C. (1990) Temperature and salinity limits for growth and survival of planktonic foraminifers in laboratory cultures. *J. Foraminiferal Res.* **20,** 128–148.

Boyle E. (1992) Cadmium and $\delta^{13}C$ paleochemical ocean distributions during the Stage 2 glacial maximum. *Ann. Rev. Earth and Planet Sci.* **20,** 245–287.

Bradshaw J. (1959) Ecology of living planktonic foraminifera in the north and equatorial Pacific Oceans. *Contrib. Cushman Found. Foraminiferal Res.* **10,** 25–64.

Broecker W. S. and Peng T.-H. (1982) *Tracers in the Sea,* pp. 306–311. Eldigeo.

Coulbourn W. T., Parker F. L., and Berger W. H. (1980) Faunal and solution patterns of planktonic foraminifera in surface sediments of the North Pacific. *Mar. Micropaleontol.* **5,** 329–399.

DeNiro M. and Epstein S. (1978) Influence of diet on the distribution of carbon isotopes in animals. *Geochim. Cosmochim. Acta* **42,** 495–506.

Deuser W. G. (1987) Seasonal variation in isotopic composition and deep-water fluxes of the tests of perennially abundant planktonic foraminifera of the Sargasso Sea: Results from sediment-trap collections and their paleoceanographic significance. *J. Foraminiferal Res.* **17,** 14–27.

Epstein S., Buchsbaum R., Lowenstam H. A., and Urey H. C. (1953) Revised carbonate-water isotopic temperature scale. *Bull. Geol. Soc. Amer.* **64,** 1315–1326.

Erez J. and Luz B. (1983) Experimental paleotemperature equation for planktonic foraminifera. *Geochim. Cosmochim. Acta* **47,** 1025–1031.

Gordon L. I., Jennings J. C., Jr., Ross A. A., and Krest J. M. (1994) A suggested protocal for continuous flow automated analysis of seawater nutrients (phosphate, nitrate, nitrite and silicic acid) in the WOCE Hydrographic Program and the Joint Global Ocean Fluxes Study. WOCE Operations Manual, WHP Office Report WHPO 91-1, WOCE Report No. 68/091, Revision 1.

Heinbokel J. F. (1978) Studies on the functional role of tintinnids in the southern California Bight, 1, Grazing and growth rates in laboratory cultures. *Mar. Biol. Berlin* **47,** 177–189.

Hemleben C., Spindler M., and Anderson O. R. (1988) *Modern Planktonic foraminifera.* Springer-Verlag.

Hickey B. (1989) Patterns and processes of circulation over the Washington continental shelf and slope. In *Coastal Oceanography of Washington and Oregon* (ed. M. Landry and B. Hickey), pp. 41–115. Elsevier Press.

Kenyon K. E. (1978) The Shallow Salinity Minimum of the eastern North Pacific in winter. *J. Phys. Oceanogr.* **8,** 1061–1069.

Kroopnick P. (1974) Correlations between ^{13}C and ΣCO_2 in surface waters and atmospheric CO_2. *Earth Planet. Sci. Lett.* **22,** 397–403.

Levitus S. (1982) Climatological atlas of the world ocean. Natl. Ocean. Atmos. Admin. Prof. Paper 13.

Lohmann G. P. (1992) Increasing seasonal upwelling in the subtropical south Atlantic over the past 700,000 yrs: Evidence from deep-living planktonic foraminifera. *Mar. Micropaleontol.* **19,** 1–12.

Lohmann G. P. and Schweitzer P. N. (1990) *Globorotalia truncatulinoides'* growth and chemistry as probes of the past thermocline: 1, Shell size. *Paleoceanogr.* **5,** 55–75.

McConnaughey T. (1989a) ^{13}C and ^{18}O isotopic disequilibrium in biological carbonates, I, Patterns. *Geochim. Cosmochim. Acta* **53,** 151–162.

McConnaughey T. (1989b) ^{13}C and ^{18}O isotopic disequilibrium in biological carbonates, II, In-vitro simulations of kinetic isotope effects. *Geochim. Cosmochim. Acta* **53,** 163–171.

McConnaughey T. A. and Whelan J. F. (1996) Calcification generates protons for nutrients and bicarbonate uptake. *Earth Sci. Rev.* (in press).

McConnaughey T. A., Burdett J., and Whelan J. F. (1996) Respiration and photosynthesis: Effects on the carbon-13 content of biological carbonates. *Geochim. Cosmochim. Acta* (submitted).

Miles G. A. (1973) Living planktonic foraminifera in the northeast Pacific Ocean, Univ. of Oregon M.A. thesis, Univ. Oregon Press.

Ortiz J. D., Mix A. C., and Collier R. W. (1995) Environmental control of living symbiotic and asymbiotic planktonic foraminifera in the California Current. *Paleoceanography* **10,** 987–1009.

Ortiz J. D., Mix A. C., and Wheeler P. (1996) An estimate of the anthropogenic $\delta^{13}C_{DIC}$ offset based on the ventilation of the California Current. *Global Biogeochem. Cycles* (in press).

Pak H., Kiefer D. A., and Kitchen K. C. (1988) Meridional variations in the concentration of chlorophyll and microparticles in the North Pacific Ocean. *Deep-Sea Res. Part A* **35,** 1151–1171.

Qiu B. (1995) Why is the spreading of the North Pacific Intermediate Water confined on density surfaces around σ_θ = 26.8? *J. Phys. Oceanogr.* **25,** 168–180.

Rau G. H., Mearns A. J., Young D. R., Olson R. J., Schafer H. A., and Kaplan I. R. (1983) Animal $^{13}C/^{12}C$ correlates with trophic level in pelagic food webs. *Ecology* **64,** 1314–1318.

Ravelo A. C. and Fairbanks R. G. (1992) Oxygen isotopic composition of multiple species of planktonic foraminifera: Recorders of the modern photic zone temperature gradient. *Paleoceanography* **7,** 815–831.

Reid J. L. (1973) The Shallow Salinity Minima of the Pacific Ocean. *Deep-Sea Res.* **20,** 51–68.

Roemmich D. and McCallister T. (1989) Large scale circulation of the North Pacific Ocean. *Prog. Oceanog.* **22,** 171–204.

Romanek C. S., Grossman E. L., and Morse J. W. (1992) Carbon isotopic fractionation in synthetic aragonite and calcite: Effects of temperature and precipitation rate. *Geochim. Cosmochim. Acta* **56,** 419–430.

Sautter L. and Thunell R. (1989) Seasonal succession of the planktonic foraminifera: Results from a four year time-series sediment trap experiment in the northern Pacific. *J. Foraminiferal Res.* **19,** 253–267.

Schmidt-Nielsen K. (1985) *Animal Physiology: Adaptation and Environment, 3rd ed.* Cambridge Univ. Press.

Schweitzer P. N. and Lohmann G. P. (1991) Ontogeny and habitat of modern Menardiiform planktonic foraminifera. *J. Foraminiferal Res.* **21,** 332–346.

Sherr B. F., Sherr E. B., and Berman T. (1983) Grazing, growth and ammonium excretions rates of a heterotrophic microflagellate fed with four species of bacteria. *Appl. Environ. Microbiol.* **45,** 1196–1201.

Spero H. J. (1988) Ultrastructural examination of chamber morphogenesis and biomineralization in the planktonic foraminifer *Orbulina universa*. *Mar. Biol. Berlin* **99,** 9–20.

Spero H. J. and Lea D. W. (1993) Does the carbon isotopic composition of planktonic foraminifera prey affect shell $\delta^{13}C$ values? *Eos Trans. AGU* **74,** 183. (abstr.)

Spero H. J. and Lea D. W. (1996) Experimental determination of stable isotope variability in Globigerina bulloides: Implications for paleoceanographic reconstructions. *Mar. Micropaleontol.* **28** (in press).

Strom S. L. (1991) Growth and grazing rates of the herbivorous dinoflagellate *Gymnodinium* sp. from the open subarctic Pacific Ocean. *Mar. Ecol. Prog. Ser.* **78,** 103–113.

Talley L. D. (1985) Ventilation of the subtropical North Pacific: The Shallow Salinity Minimum. *J. Phys. Oceanogr.* **15,** 633–649.

Talley L. D. (1991) An Okhotsk Sea water anomaly: Implications for ventilation in the North Pacific. *Deep-Sea Res.* **38,** 171–190.

Talley L. D. (1993) Distribution and formation of the North Pacific Intermediate Water. *J. Phys. Oceanogr.* **23,** 517–537.

Talley L. D., Joyce T. M., and de Szoeke R. A. (1991) Transpacific sections at 47°N and 152°W: Distribution of properties. *Deep-Sea Res.* **38,** 63–82.

Thomson R. E. and Papadakis J. E. (1987) Upwelling filaments and motion of a satellite-tracked drifter along the west coast of North America. *J. Geophys. Res.* **92,** 6445–6461.

Van Scoy K. A. and Druffel E. R. M. (1993) Ventilation and transport of the thermocline and intermediate waters in the Northeast Pacific during recent El Niños. *J. Geophys. Res.* **98,** 18,083–18,088.

Van Scoy K. A., Olson D. B., and Fine R. A. (1991) Ventilation of the North Pacific Intermediate Waters: The role of the Alaskan Gyre. *J. Geophys. Res.* **96,** 16801–16810.

Vergnaud Grazzini C. (1976) Nonequilibrium isotopic compositions of shells of planktonic foraminifera in the Mediterranean Sea. *Palaeogeogr. Palaeoclimatol. Palaeoecol.* **20,** 263–276.

Verity P. (1991) Measurement and simulation of prey uptake by marine planktonic cilliates fed plastidic and aplastidic nanoplankton. *Limnol. Oceanogr.* **36,** 729–750.

Vinot-Bertouille A.-C. and Duplessy J.-C. (1973) Individual isotopic fractionation of carbon and oxygen in benthic foraminifera. *Earth Planet. Sci. Lett.* **18,** 247–252.

Wiebe P. H. et al. (1985) New developments in the MOCNESS, an apparatus for sampling zooplankton and micronekton. *Mar. Biol. Berlin* **87,** 313–323.

Williams D. F., Bé A. W. H., and Fairbanks R. G. (1981) Seasonal stable isotopic variations in living planktonic foraminifera from Bermuda plankton tows. *Palaeogeogr. Palaeoclimatol. Palaeoecol.* **33,** 71–102.

Yuan X. and Talley L. D. (1992) Shallow Salinity Minima in the North Pacific. *J. Phys. Oceanogr.* **22,** 1302–1316.

Zahn R., Pedersen T. F., Bornhold B. D., and Mix A. C. (1991) Water mass conversion in the glacial subarctic Pacific (54°N, 148°W): Physical constraints and the benthic-planktonic stable isotope record. *Paleoceanography* **6,** 543–560.

Zaneveld J. R., Spinrad R. W., and Bartz R. (1979) Optical properties of turbidity standards. *Ocean Optics VI. Proc. SPIE Int. Soc. Opt. Eng.* **208,** 159–168.